

Geophysical Research Letters

RESEARCH LETTER

10.1029/2020GL088693

Key Points:

- The majority of thermal crack damage is produced during heating in the coarse-grained granophyre but during cooling in the finer-grained andesite and basalt
- A temperature-memory effect is exhibited during thermal cycling in the quartz-rich granophyre but not in the quartz-poor andesite or basalt
- Interpretation of prefailure seismicity in volcanic/geothermal settings needs to take account of damage accumulated in earlier deformation cycles

Supporting Information:

- Supporting Information S1

Correspondence to:

J. Browning,
jrbrowning@ing.puc.cl

Citation:

Daoud, A., Browning, J., Meredith, P. G., & Mitchell, T. M. (2020). Microstructural controls on thermal crack damage and the presence of a temperature-memory effect during cyclic thermal stressing of rocks. *Geophysical Research Letters*, 47, e2020GL088693. <https://doi.org/10.1029/2020GL088693>

Received 1 MAY 2020
Accepted 21 SEP 2020

Microstructural Controls on Thermal Crack Damage and the Presence of a Temperature-Memory Effect During Cyclic Thermal Stressing of Rocks

Ali Daoud¹, John Browning^{1,2,3} , Philip G. Meredith¹ , and Thomas M. Mitchell¹ 

¹Department of Earth Sciences, University College London, London, England, ²Department of Mining Engineering and Department of Structural and Geotechnical Engineering, Pontificia Universidad Católica de Chile, Santiago, Chile, ³Andean Geothermal Centre of Excellence (CEGA), Santiago, Chile

Abstract We present results from a series of thermal stressing experiments that used three igneous rocks of different composition, grain size, and origin and contemporaneously recorded acoustic emissions (AEs) with changing temperature. Samples were subjected to both a single heating and cooling cycle and multiple heating/cooling cycles to different peak temperatures. The vast majority of thermal crack damage is generated during heating in the coarser-grained (quartz rich) rock but during cooling in the two finer-grained (quartz poor) rocks. Our AE results also demonstrate the presence of a temperature-memory effect, analogous to the Kaiser stress-memory effect observed during cyclic mechanical loading, but only in the coarser-grained rock. We suggest that the total amount of crack damage induced during either heating or cooling is dependent on the mineral composition and, most importantly, the grain size and arrangement, as well as the maximum temperature to which the rock was exposed. We use our laboratory-scale results to suggest ways in which crustal-scale geophysical data may need to be reinterpreted to provide more accurate estimates of total, accumulated damage and the approach to macroscopic failure in crustal segments hosting magma chambers and geothermal reservoirs.

Plain Language Summary We present results from a series of laboratory thermal stressing experiments using three igneous rocks of different composition, grain size, and origin: a Granophyre (SGP) from the Slaufudalur pluton in Iceland, an Andesite from Santorini, Greece (SA), and a Basalt from the Seljadalur region of Iceland (SB), in which acoustic emissions (AEs) were recorded at the same time as the temperature of the samples was experimentally increased or decreased. Samples were subjected to both a single heating and cooling cycle and multiple heating and cooling cycles to different peak temperatures. The vast majority of thermal crack damage was generated during heating in the larger-grained SGP but during cooling in the smaller-grained SA and SB. Our AE results demonstrate the presence of a temperature-memory effect in SGP, analogous to the Kaiser stress-memory effect observed during cyclic mechanical loading, but no similar effect is observed in either SA or SB. We suggest that the total amount of crack damage is dependent on the mineral composition and, most importantly, the grain size and arrangement, as well as the maximum temperature to which the rock was exposed. The results should be considered in models that consider the distribution of damage in cyclically thermally stressed regions such as crustal segments hosting geothermal reservoirs and/or magmatic intrusions.

1. Introduction

Volcanic and geothermal systems commonly experience complex cyclic stressing resulting from the mechanical loading of regional tectonics or local fluid movements (Gudmundsson, 2006). While the role of cyclic mechanical stressing is still not fully understood, substantial work has been made to investigate this problem in volcanic settings (Heap et al., 2009, 2010; Heimissson et al., 2015). However, another important but much less well-studied process in these systems is that of cyclic thermal stressing. For example, brittle materials such as rocks commonly exhibit a stress memory effect, or so-called *Kaiser effect*, when cyclically deformed through mechanical loading (Browning et al., 2018; Holcomb, 1993; Kaiser, 1953; Lavrov, 2001, 2003; Lockner, 1993). This effect has been shown both in laboratory-scale rock samples (e.g., Browning et al., 2018; Heap et al., 2009) and also on the scale of kilometers regionally in parts of Iceland (Heimissson et al., 2015). Manifestation of the Kaiser effect is most commonly discerned through monitoring the

output of microseismicity or acoustic emissions (AEs) as a proxy for induced crack damage. In the laboratory rock deformation experiments of Lockner (1993) and Heap et al. (2009), it was noted that AE only commenced on any loading cycle once the maximum stress in the preceding cycle was reached or exceeded. Browning et al. (2017) expanded on this observation to suggest that it is not the individual stress state that controls the AE onset level but instead the crack damage state, and hence, the Kaiser effect is actually a damage memory effect rather than a stress memory effect. Browning et al. (2018) used a true-triaxial apparatus to extend this observation further and suggest that materials can exhibit multiple damage memories depending on the relative orientations of the principal stresses and also the stressing history. As such, mechanical cyclic loading is relatively well studied and understood. By contrast, however, damage processes related to temperature cycling have received significantly less attention and are therefore less well understood. Hence, the processes that operate during cyclic thermal stressing remain enigmatic, and the sparse observations from cyclic thermal stressing experiments that have been performed to date remain inconclusive (e.g., Heap et al., 2013). The problem is further compounded by the paucity of geophysical data related to cyclic thermal damage in natural crustal settings. Hence, while cyclic thermal damage likely contributes to natural seismicity in regions that experience temperature changes, the nature of the cyclic crack damage forming processes remains enigmatic. Studies of single-cycle thermal cracking experiments that have combined laboratory data with modeled geothermal reservoirs have however shown that thermal damage can significantly change both the physical and transport properties of rocks (i.e., Sepúlveda et al., 2020; Siratovich et al., 2015). These changes, which are cyclic in nature, may therefore influence both failure related processes and the interpretation of seismic or modeled data.

Historically, the vast majority of studies of thermal cracking in rocks have concentrated primarily on the heating cycle (Meredith et al., 2001; Richter & Simmons, 1974; Simmons & Cooper, 1978; Vinciguerra et al., 2005) and so could only deduce thermal cracking during heating and not during cooling. However, more recent studies of thermal cracking in poly-crystalline rocks have presented evidence to suggest that substantial amounts of thermal cracking are generated during cooling (Browning et al., 2016; Castagna et al., 2018; Heap et al., 2013; Mollo et al., 2013). In contrast, the thermal stressing experiments of Griffiths et al. (2018), where ultrasonic velocities and acoustic emissions were recorded both during the heating and cooling of Westerly Granite samples, suggest that most thermal crack damage was generated during heating and that changes in seismic codas during cooling resulted from grain sliding and rearrangement and not from further thermal cracking. It is therefore important to reconcile these apparently contradictory observations.

Here we report results from a suite of thermal stressing experiments on three different igneous rocks, conducted under identical conditions and using the same experimental arrangement. The rocks were chosen because they represent a range of different mineralogies and microstructures. The experiments were designed to test ideas on the magnitude and frequency of thermal cracking during both heating and cooling, as well as during cyclic thermal stressing. As such, we performed both single-cycle heating and cooling experiments and multiple-cycle heating and cooling experiments. We made contemporaneous measurements of AE output throughout each experiment, with the AE acting as a proxy for the relative size and number of microcracks formed during thermal stressing.

2. Experimental Material

Three intrusive igneous rocks were selected for our thermal stressing tests (Figure 1). A coarse-grained granophyre from the Slaufudalur pluton in Eastern Iceland (SGP) (Browning et al., 2016; Burchardt et al., 2012), a bimodal grain-sized andesite from Santorini (SA), and a finer grained basalt from the Seljadalur region of SW Iceland (SB). SGP is an intrusive granophyre from a pluton, with an initial porosity of around 2% (Browning et al., 2016). The microstructure of SGP is dominated by >1 mm interlocked quartz grains. SA is an intrusive andesite from a dyke, with a relatively high initial porosity of around 13%, comprised of primarily open vesicular pores with some preexisting microcracks that primarily emanate from vesicle boundaries. The microstructure of SA comprises large (>0.5 mm) plagioclase crystals embedded within a much finer-grained matrix of plagioclase and pyroxene. SB is an intrusive, tholeiitic basalt (a sill), with an initial porosity of around 4% (Browning et al., 2016; Vinciguerra et al., 2005). Its microstructure is dominated by an intergranular matrix of plagioclase, granular pyroxene, and iron oxides. Partially oriented plagioclase

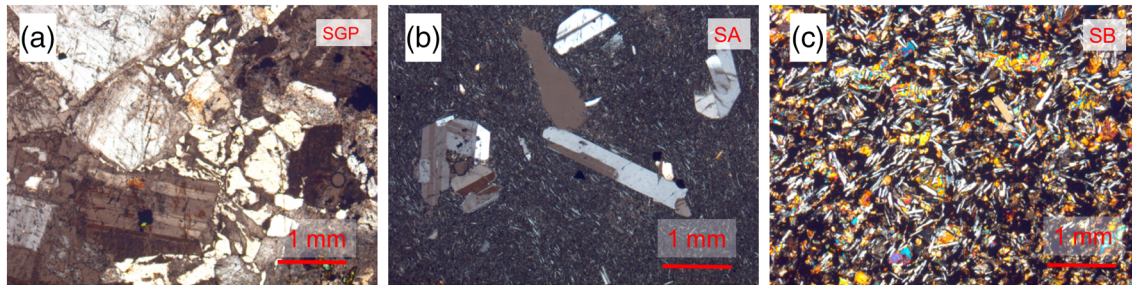


Figure 1. The three materials studied (a) granophyre from eastern Iceland (SGP), (b) andesite from Santorini, Greece (SA), and (c) basalt from Seljadalur Iceland (SB). SGP is dominated by >1 mm interlocked quartz grains, whereas SA has a very fine-grained Plg/Px matrix with larger (>0.5 mm) plagioclase crystals embedded. SB consists of plagioclase laths within a finer-grained matrix of Ol/Px crystals.

is also found, along with a rare abundance of augite, olivine, and an interstitial glass phase. The SB used in this study was very similar to that used by Nara et al. (2011) and Vinciguerra et al. (2005) who both report the absence of visible preexisting microfractures. We also could not observe preexisting microfractures in our starting material.

3. Experimental Setup

Core samples, measuring 25 mm in diameter by 65 mm in length, were held within a purpose-built heating jig manufactured from 310 stainless steel alloy, capable of sustaining temperatures up to 1100°C without significant corrosion. The jig is approximately 1 m in length and comprises a series of rods and springs to hold the sample under constant end-load within the central, uniform temperature section, of a Carbolite CTF12/75/700 tube furnace while allowing for expansion and contraction (Figure 2) (see also Browning, 2015; Browning et al., 2016; Castagna et al., 2018). The central rods act as acoustic waveguides and are of sufficient length to enable the AE transducer to be located outside of the furnace where it remains cool. The external springs allow the central rods to move in response to sample expansion and contraction during heating and cooling and therefore maintain a uniform contact throughout the experiments. Temperature was monitored by a thermocouple placed on the sample surface and controlled using a calibrated thermocouple contained within the tube furnace. All experiments were conducted at ambient pressure.

4. Experimental Protocol

Below, we present results from two suites of thermal stressing tests. In the first suite, samples of each rock type were individually subjected to a single heating and cooling cycle to a maximum temperature of 900°C. In these tests, the samples were heated at a rate of 1°C/min, held at the maximum temperature for 30 min, and then cooled at a natural cooling rate that did not exceed 1°C/min. In the second suite, samples were subjected to multiple heating and cooling cycles to peak temperatures of 350°C, 500°C, 700°C, and

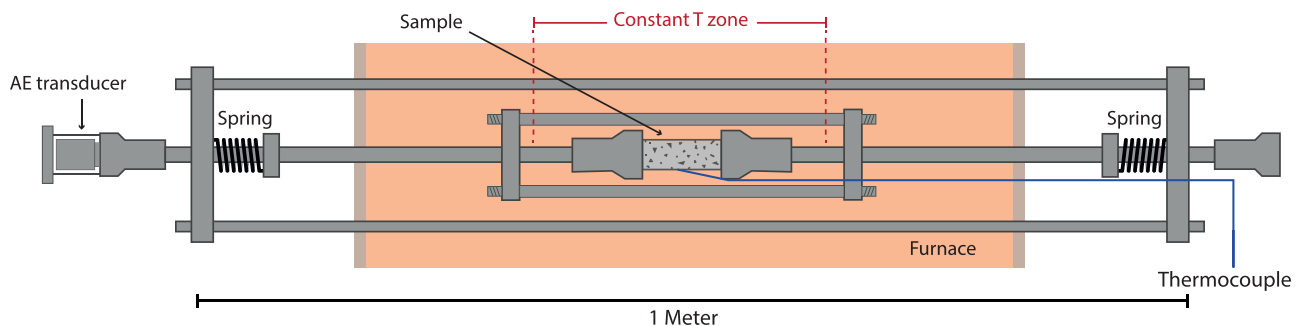


Figure 2. Schematic diagram of the experimental arrangement used for the cyclic thermal stressing experiments (modified after Browning et al., 2016).

900°C (all at a constant rate of 1°C/min on heating and a natural cooling rate of <1°C/min). The samples were held at each peak temperature for 30 min, which was found to be sufficient time for thermal equilibration (see Browning et al. [2016] for further details). In order to capture dynamic crack growth and nucleation events during the tests, we recorded acoustic emissions contemporaneously during each test using a Panametrics V103 piezoelectric *P* wave transducer attached to one end of the wave guide. The signal was pre-amplified and recorded using a Vallen AMSY-5 acoustic emission analyzer. The preamplifier was set with a fixed gain of 30 dB and a detection threshold of 40 dB. Importantly, the settings of the AE instrumentation were identical for all tests so that the AE data are comparable between tests. Arrival times were used to calculate the AE hit rate, which we use as a contemporaneous measure for the rate of cracking. The area under the envelope of each discrete waveform is used to measure the relative energy associated with each AE hit which we use as a proxy to estimate the relative size of crack growth increments. Additionally, we also measured the *P* wave velocities of our rock samples prior to and after each heating and cooling cycle (the data are provided in the supporting information). Together, these measurements provide insights into the total amount of crack damage formed during the combined heating and cooling cycles.

5. Results

5.1. Single Heating and Cooling Cycle Tests

In Figure 3, we plot the cumulative number of AE hits, energy output, and temperature as functions of time for thermal stressing tests on each rock type heated to 900°C and then cooled back to ambient temperature in a single cycle. In the test on Slaufudalur Granophyre (SGP), both the cumulative number of AE hits and the AE energy output are notably higher during the heating phase than during the cooling phase (Figures 3a and 3d). In total, some 83,000 AE hits were recorded, and over 72,000 (87%) of these were generated during the heating phase (Table 1). We observe comparable results for the output of AE energy (88% generated during the heating phase) and also note that the AE energy per hit is very similar for hits generated in both the heating and cooling phases (Table 1).

By contrast, the output of AE for both Santorini Andesite (SA) and Seljadalur Basalt (SB) is much greater during the cooling phases than during the heating phases (Figures 3b, 3c, 3e, and 3f and Table 1). For SA, a total of just over 7,000 AE hits are generated during the whole test, with over 90% being generated during the cooling phase (Table 1). Similarly, well over 90% of the AE energy is generated during this phase. However, we also note that the AE energy per hit is higher by about a factor of four for the AE hits generated during cooling than for those generated during heating. A similar pattern is observed for SB, with over 90% of the 6,000 recorded AE hits and over 90% of the AE energy being generated during the cooling phase (Table 1). Once again, we note that the AE energy per hit is significantly higher (by approximately a factor of 2) for hits generated during the cooling phase.

5.2. Multiple Heating and Cooling Cycle (Thermal Cycling) Tests

In Figure 4, we present results from the suite of multiple cycle, thermal cycling tests on each rock type. In these tests, each sample was subjected to four heating and cooling cycles to successively increasing peak temperatures of 350°C, 500°C, 700°C, and 900°C. Again, we plot cumulative AE hits and AE energy output against temperature and as functions of time. However, we also mark, for each rock type, the onset of AE output during each of the heating phases where AE was generated. In the test on SGP (Figures 4a and 4d), we observe essentially no AE output during either the heating or cooling phases of the first cycle to a temperature peak of 350°C. By contrast, during the second heating cycle, we observe the onset of significant AE output around 380°C, which continues at a relatively constant rate until the temperature peak of 500°C is reached. We then observe essentially zero AE output during the cooling phase of this cycle (Figures 4a and 4d). We also note that during the third heating cycle the AE output recommenced at 500°C, significantly higher than the onset temperature of 380°C in the previous cycle. Significantly, this corresponds both to the maximum temperature in the previous cycle and the point at which AE output ceased during that cycle. This observation suggests the presence of a “temperature-memory” effect, analogous to the Kaiser stress memory effect reported in numerous studies of cyclic mechanical loading of rocks (Browning et al., 2018; Holcomb, 1993; Lavrov, 2001, 2003; Lockner, 1993). The AE output continued to increase steadily until the temperature peak of 700°C was reached. A relatively small amount of AE output occurred during the very earliest part of the cooling phase but ceased after that, with essentially nothing being recorded

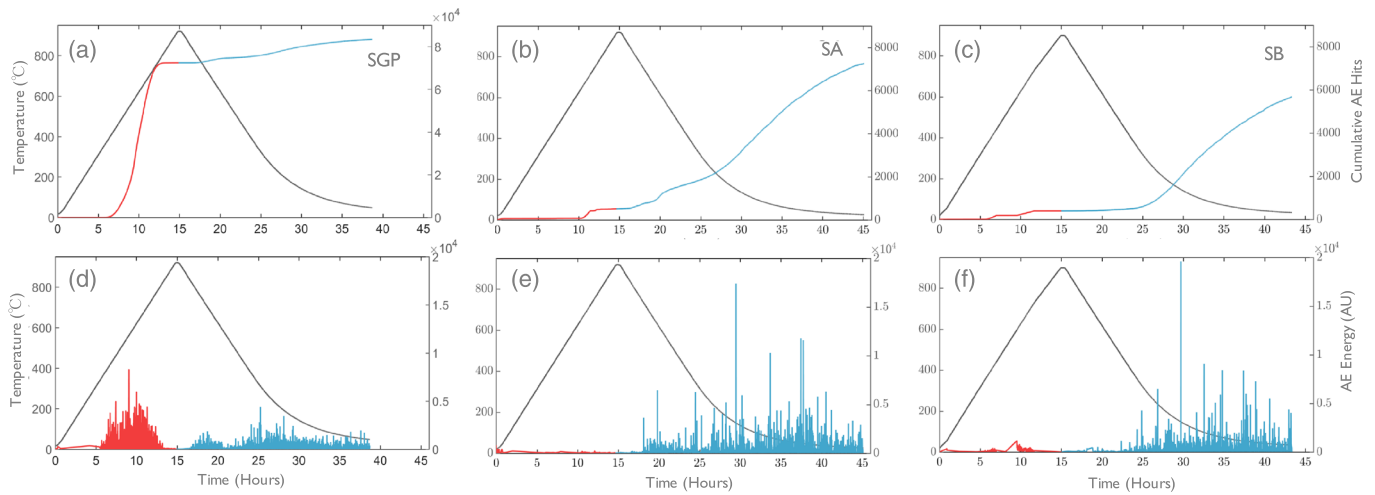


Figure 3. Cumulative acoustic emission hits generated during heating (in red) and cooling (in blue) from 900°C in the three rock types, (a) Slaufudalur Granophyre (SGP), (b) Santorini Andesite (SA), and (c) Seljadalur Basalt (SB) with acoustic emission hit energy recorded in (d)–(f). NOTE: Order of magnitude difference in AE totals between SGP (a and d) and SA/SB (b, c, e, and f).

during the remainder of the cooling phase. A similar pattern of activity was observed during the final cycle, with the heating being essentially aseismic until a temperature of 680°C was reached. This is close to the previous maximum temperature and also corresponds to the temperature at which AE ceased during the cooling phase of the previous cycle. This observation therefore adds further support to the idea of a temperature-memory effect in SGP. We again observed very little AE output during the initial phase of cooling from the maximum temperature of 900°C, but we did observe a significant output of AE at temperatures below 500°C, during the final phase of cooling in this cycle. In total, around 50,000 AE hits were generated over the four cycles of heating and cooling; somewhat fewer than the >80,000 generated during heating to the same maximum temperature during a single cycle (Figure 3a and Table 1).

The results from the thermal cycling tests on both SA (Figures 4b and 4e) and SB (Figures 4c and 4f) were very similar to each other but quite different from those for Slaufudalur Granophyre, although all three rocks were exposed to identical thermal cycling to the same set of peak temperatures. During the thermal cycling test on SA we recorded no significant AE during the first two cycles of heating and cooling to peak temperatures of 350°C and 500°C. The first onset of AE output occurs around 600°C during the heating phase of the third cycle, but both the number of hits and the energy are rather low. Significantly more AE is generated during the phase of cooling from the temperature peak of 700°C. During the final cycle, we again observe an AE onset at the same temperature of 600°C during the heating phase, and the output continues up to the maximum temperature of 900°C. Again, we observe that the great majority of the AE output, both in terms of the number of hits and the energy, is generated during the phase of cooling from the maximum temperature. In fact, more than 75% of the AE hits and more than 85% of the AE energy were generated during this single, final cooling phase. Furthermore, the observation that the AE onsets during the

Table 1

Summary of AE Outputs (Cumulative AE Hits, Cumulative AE Energy and Energy/Hit) Generated During the Heating and Cooling Phases of the Single Thermal Cycling Tests on Slaufudalur Granophyre (SGP), Santorini Andesite (SA), and Seljadalur Basalt (SB)

Rock (phase)	\sum AE hits		\sum AE energy		Energy/hit
SGP (Heating)	72,428	87%	10.1×10^6	88%	139
SGP (Cooling)	10,873	13%	1.34×10^6	12%	123
SA (Heating)	517	7%	0.03×10^6	2%	58
SA (Cooling)	6,745	93%	1.32×10^6	98%	198
SB (Heating)	468	7%	0.06×10^6	6%	121
SB (Cooling)	5,292	93%	1.06×10^6	94%	200

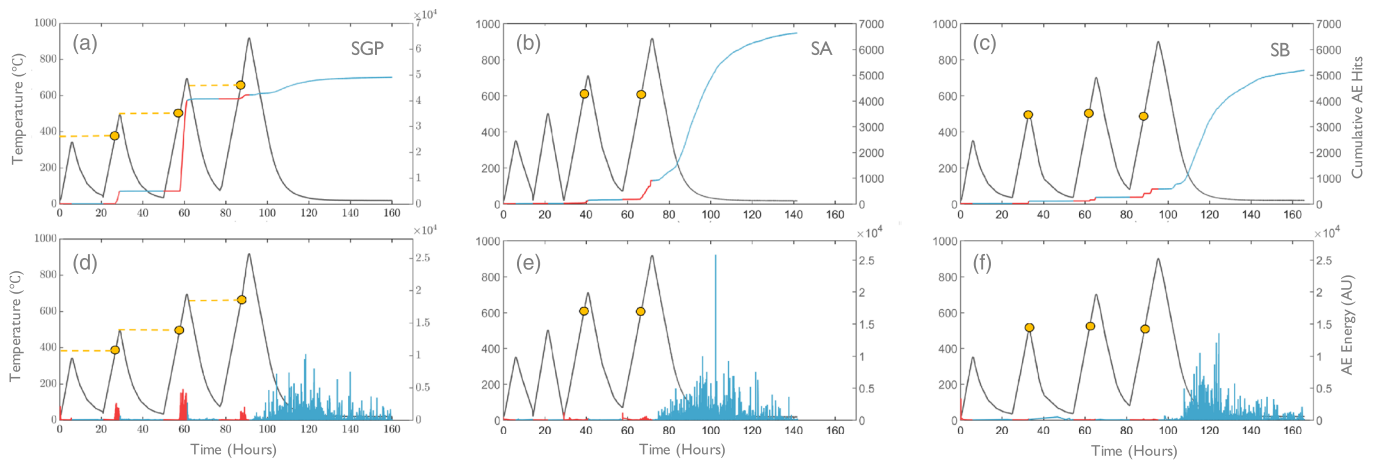


Figure 4. Cumulative AE hits (a–c) and AE energy (d–f) generated during multiple cyclic heating (in red) and cooling (in blue) to peak temperatures of 350°C, 500°C, 700°C, and 900°C in Slauchudalar Granophyre (SGP), Santorini Andesite (SA), and Seljadalar Basalt (SB), respectively. Orange dots indicate the onset of AE output in each cycle where significant AE was generated. Note the order of magnitude difference in the scale of cumulative AE hits between SGP (a) and SA/SB (b and c).

third and fourth heating phases occurred at the same temperature suggests that there was no manifestation of any temperature-memory effect in the Santorini Andesite.

A broadly similar pattern of activity is observed in the thermal cycling test on SB. We observe no AE output during either the heating or cooling phases of the first cycle to a temperature peak of 350°C. The first onset of AE output commenced around 500°C, very close to the temperature peak in the second cycle. As for SA, we note that the AE onsets for SB commence at the same temperature of 500°C during the heating phases of both cycles three and four. This again suggests that SB, just like SA, exhibits no manifestation of any temperature-memory effect. Also like SA, we note that significantly more AE output was generated during the cooling phase of each cycle than during the heating phases, with approximately 90% of the AE hits and 90% of the AE energy being generated during the single, final phase of cooling from 900°C.

By contrast with SGP, the total number of AE hits generated during the four cycles of the thermal cycling tests on both SA and SB was broadly similar to the total number generated during the single cycle tests (differences of around 6%) (Figures 3b and 3c and Table 1).

We also measured radial P wave velocities (V_p) on all of the as received rocks and repeated the measurements after each heating and cooling cycle (supporting information). The change in V_p following heat treatment was most notable in SGP where the initial average velocity of 4.8 km s⁻¹ decreased with every temperature step to a minimum of 1.7 km s⁻¹ after the highest temperature of 900°C, a change of 64%. Similarly, SB also experienced decreases in V_p with each temperature step, starting at 5.4 km s⁻¹ and decreasing to 3.6 km s⁻¹, a change of 33%. The change in V_p for SA was less but still significant, decreasing from 4.6 to 4.3 km s⁻¹, a change of 7%.

6. Discussion

Our experimental results demonstrate clearly that the AE behavior of SGP during thermal stressing is fundamentally different from that of both SA and SB, whereas the patterns of behavior of SA and SB are essentially the same. This occurs even though all three rocks were subjected to identical heating and cooling regimes to identical peak temperatures using the same experimental apparatus. Since we use the output of AE in these experiments as a proxy for the generation of thermal crack damage within our samples, the results suggest that the pattern of thermal crack damage generated during heating and cooling of SGP, SA, and SB is also very different. One apparently obvious way that could normally be used to verify this, at least qualitatively, would be via post mortem microstructural analysis of the crack fabrics. However, as we have noted previously (Browning et al., 2016), a major problem when studying thermal cracking induced by both heating and cooling is that we can only observe a palimpsest of the data because any cracking

induced during heating is overwritten by the cracking induced during cooling. This issue becomes even more dominant where multiple heating and cooling cycles are involved. It is therefore impossible to discriminate at what point during the tests the cracks were generated from any postmortem analysis. Similarly, our pretest and posttest measurements of P wave velocities can be used to discern the total amount of induced thermal crack damage during any test but cannot be used to distinguish between damage induced during the heating part and damage induced during the cooling part of any cycle. Reliable interpretation is therefore dependent on analysis of the AE data which is recorded contemporaneously with changes in temperature in real time.

First, as noted above, the total number of AE hits and level of AE energy generated during the heating of SGP to 900°C and cooling back to ambient temperature is about an order of magnitude higher than for either SA or SB (Figure 3 and Table 1). This implies that much more thermal crack damage is generated in SGP than SA or SB during these single cycle heating and cooling tests. Second, the very different proportions of AE generated during the heating and cooling phases for the different materials (Table 1) suggest that most thermal crack damage is generated during the heating phases in SGP and during the cooling phases in SA and SB. Third, we note that the AE energy per hit was essentially the same for both the heating and cooling phases of the test on SGP (Table 1). The AE energy for any hit is defined as the area under the amplitude-time envelope and is therefore a measure of the size of the hit (Cox & Meredith, 1993). This implies, therefore, that the mean size of the thermally induced cracks in both phases was also essentially the same for SGP. By contrast, for both SA and SB, the AE energy per hit was significantly higher during the cooling phase than during the heating phase, implying that, not only were more cracks generated during cooling than during heating in these rocks but also that their average size was larger. Finally, in our thermal cycling tests, we observe a temperature-memory effect in SGP, whereby new AE output (and, hence, new crack growth) only commences when the peak temperature in the previous cycle is equaled or exceeded (Figure 4a). By contrast, no such temperature memory was observed during the cyclic tests on either SA or SB; rather, AE output commenced at the same temperature during each heating phase (Figures 4b and 4c).

Our complementary measurements of P wave velocities are broadly consistent with this interpretation of the AE data. As noted earlier, we measured the P wave velocities of our all of our “as received” samples before testing and then measured them again after each heating and cooling cycle to 350°C, 500°C, 700°C, and 900°C (details are given in the supporting information). For SGP, the mean P wave velocity decreased by 64%, from 4.8 to 1.7 km s⁻¹ after heat treatment to 900°C. We measured a smaller decrease of 33% for SB from 5.4 to 3.6 km s⁻¹. Finally, the mean velocity in SA decreased by only about 7%, from 4.6 to 4.3 km s⁻¹. Most noticeably, the reductions in the P wave velocities demonstrate that significantly more thermal crack damage is induced in SGP than in either SA or SB over the same temperature range. The differences in P wave velocity change between SA and SB can be explained by the materials different initial porosities. SA has a very high initial porosity of 13%, whereas SB has a lower initial porosity of 4%. Hence, in the high porosity SA, even a substantial amount of thermal crack damage will not increase the porosity (i.e., total void volume) significantly. The change in P wave velocity following heat treatment responds to the relative change in total void volume. In a high porosity rock, it is therefore possible to get a high level of AE output generated by thermal cracking without significantly changing the P wave velocity. Vinciguerra et al. (2005) showed that the P wave velocity of Icelandic basalt with an initial porosity of around 1% decreased by around 40% after heating to 900°C, whereas the P wave velocity of basalt from Mt. Etna, with a porosity >2% and a very high initial crack density, decreased by less than 1% after heating to the same temperature. It is therefore not at all surprising that our samples of SA, with an initial porosity of around 13%, showed only a marginal decrease in P wave velocity after thermal treatment.

So, how can we explain the apparently contradictory observations of a temperature memory effect in SGP but none in SB and SA? Given that the sample dimensions were identical, the experimental protocols were identical and all tests were conducted using the same experimental apparatus, we look to the compositions of the three different rocks.

SGP is a tightly packed, coarse-grained rock with a microstructure dominated by interlocking quartz grains. It is well known that the thermal expansion coefficients of quartz are highly anisotropic, with the a axis value being around 1.6 times the c axis value at ambient temperature (Nye, 1957), and increasing with temperature to around 1.75 at 270°C (Meredith et al., 2001). It therefore seems reasonable to suggest that

the thermal expansion anisotropy is likely to be around 2 at least for the temperatures of this study. Meredith et al. (2001) reported that, for heating of a quartz-rich rock with randomly oriented grains, the expansion of each grain is partially constrained by the attempted expansion of its neighboring grains; and termed this the *internal self-constraint*. This self-constraint leads to thermal strain deficits in the high-expansion a direction and small thermal strain excesses in the low-expansion c direction, maintained by the generation of anisotropic thermal stresses. They therefore concluded that the mechanism responsible for thermal cracking in quartz-rich rocks is most likely to be splitting of individual grains due to the compressive stress generated along their a axes, aided by the small tensile stress generated along their c -axes, during heating. Conversely, the low level of cracking that occurs during cooling of SGP is likely associated with grain realignment and sliding and some extension of preexisting thermal cracks during contraction, as suggested by Griffiths et al. (2018).

These explanations are entirely consistent with the main features of the AE data generated in SGP in this study; the great majority of cracking occurring during heating rather than cooling, and the occurrence of a temperature-memory effect. There have been relatively few studies of the effect of thermal cycling on crack growth in quartz-rich rocks, but Atkinson et al. (1984) performed such experiments on samples of Westerly granite. Their AE results demonstrated that the great majority of cracking occurred during heating rather than during cooling and also confirmed the earlier observations of Johnson et al. (1978) and Yong and Wang (1980) of a temperature-memory effect equivalent to the Kaiser stress-memory observed during cyclic mechanical loading. Essentially, the cracks that are generated by the thermal stresses during heating close (essentially elastically but with some realignment and sliding) during cooling and then reopen during reheating. Only when the previous maximum temperature is exceeded do the thermal stresses again become high enough to induce new crack growth.

By contrast, the microstructure of SA comprises large angular plagioclase crystals embedded within a much finer-grained matrix, while SB comprises smaller, partially oriented plagioclase crystals in a finer-grained matrix with an interstitial glass phase. We simplify this for both SA and SB by considering the phenocrysts as acting as elastic inclusions within an essentially homogeneous matrix. We can then follow the same analysis as Browning et al. (2016) and apply the model of Fredrich and Wong (1986) which analyses the effect of temperature changes on the stress field around an angular inclusion embedded within an essentially homogeneous matrix. Specifically, they obtained solutions for the tensile stress intensity factors for microfractures within and adjacent to such inclusions, taking account of both thermal expansion anisotropy within grains and thermal expansion mismatch between grains of different minerals. Their overall conclusions were that (1) for thermal expansion anisotropy, crack growth was inherently stable with both intragranular and grain boundary cracks only growing to lengths between 0.2 and 0.3 of the inclusion length before arresting, and (2) for thermal expansion mismatch, intragranular cracks again stabilized around 0.3 of the inclusion length, whereas grain boundary cracks were inherently unstable and were predicted to propagate along the whole length of the inclusion, only terminating at a geometrical discontinuity (the end of the inclusion).

Our results therefore suggest that the sparse and low energy AE events generated in SA and SB during heating are likely due to small increments of extension of preexisting grain boundary cracks and the growth of relatively small numbers of new, intragranular cracks, within an overall compressional regime. By contrast, the numerous and higher energy AE events generated during cooling are likely due to the growth of large numbers of full-length grain boundary cracks together with a significant number of intragranular cracks of more limited extent, within an overall tensile regime. The same conclusions were drawn by Browning et al. (2016) when applying the Fredrich and Wong (1986) model to single heating and cooling cycle tests on Seljadalur basalt and Nea Kameni dacite. Since our interpretation is that very few and only partial, cracks are induced during heating in SA and SB, large numbers of potential crack nucleation and extension sites remain. It is therefore not surprising that cracking can recommence at these sites at the same onset temperature (and same thermally induced stress) in subsequent heating phases during multiple thermal cycling tests (Figures 4b and 4c).

As noted above, like the AE data, the P wave velocity data also show that significantly more thermal crack damage is induced in SGP than in either SA or SB during temperature cycling. However, while the AE output was very similar for both SA and SB, we observe a significantly smaller reduction in P wave velocity for SA (7%) than for SB (33%). While this may initially appear counterintuitive, it is entirely as expected and

can be simply explained by the very different porosities of SA and SB. SA has an initial porosity of 13% and a P wave velocity of 4.6 km s^{-1} , while SB has a much lower porosity of only 4% and a comparably higher P wave velocity of 5.4 km s^{-1} . Therefore, the same amount of induced extra void space, in the form of thermal crack damage, would be expected to have a commensurately larger effect on the P wave velocity of the low-porosity SB than on that of the high-porosity SA. Similar complexities in thermal cracking characteristics in volcanic rocks have been documented by Griffiths (2018) and also explained through differences in the preexisting damage and initial porosities.

6.1. Implications for Cyclic Thermal Stressing and Damage in the Crust

Our results have implications for the deformation response of crustal segments that host magma chambers. Over the lifetime of any magma chamber, the surrounding country rock is likely to experience multiple cycles of both mechanical and thermal stressing. Such stresses are initially generated by magma emplacement, whereby accommodation of any new volume of magma elevates the level of normal (mechanical) stress and generates thermal stress by transfer of heat from the magma to the country rock (Gudmundsson, 2006). Over time, the magma chamber may cool and deflate, thus reducing the level of normal stress and inhibiting further mechanical damage (Heap et al., 2010) but continuing to generate thermal stress and thermally induced damage. We have shown that the extent of thermal damage during cooling is highly dependent on the microstructure of the rock, whereby coarse-grained, quartz-rich rocks, such as granophyre will experience relatively low amounts of thermal damage during cooling, while finer grained, quartz-poor rocks, such as basalt and andesite, experience much higher levels. Any such cooling and deflation of the chamber is likely to be punctuated by further periods of magma replenishment and chamber inflation. This highly cyclical behavior leads to repeated occurrences of both mechanical and thermal stressing of the surrounding country rock.

It has previously been shown that many crustal rocks exhibit a Kaiser stress-memory effect when cyclically mechanically loaded (Heap et al., 2010; Holcomb., 1993; Lavrov, 2003). The occurrence of a Kaiser effect has profound implications for the interpretation of remotely monitored seismic data and understanding the approach to failure of stressed crustal segments and, in the case of volcanic systems, eventual eruption. That is because the induced damage is cumulative over all cycles, while seismicity only records the contemporary damage generated during the current cycle. Therefore, reliance on seismicity alone is likely to severely underestimate the total accumulated damage and, hence, the proximity to failure. Like mechanically induced damage (Benson et al., 2020), thermally induced damage is also known to alter rock properties such as strength and stiffness (Heap et al., 2013; Kendrick et al., 2013; Siratovich et al., 2015). Hence, thermal cracking is also likely to influence both the amount of deformation in volcanic settings and the eventual onset of failure. However, to date there has been no dedicated geophysical study focused on the relative contributions of thermal damage and mechanical damage to the failure process, although seismic events related to the cooling of magmatic systems have been interpreted (Miller et al., 1998). Nevertheless, Browning et al., (2016) raised the potential for a quantitative link between laboratory-scale measurements and crustal-scale observations by comparing the frequencies of laboratory AE signals ($\sim 1 \text{ MHz}$) with those of natural seismic signals at volcanoes ($\sim 1\text{--}5 \text{ Hz}$) and the relative fracture lengths at both scales through the well-established frequency-length scaling law of Aki and Richards (1980). Hence, it remains a priority in physical volcanology to measure simultaneously the fracture length and frequency associated with seismic signals generated during thermal cracking events in crustal segments hosting volcanoes or geothermal reservoirs. Furthermore, the interpretation of natural seismicity within the context of failure forecasting models (e.g., Bell et al., 2011) may need to be amended, depending on whether the region of study demonstrates a temperature memory effect or not, which, as our results have demonstrated, is at least partially controlled by rock type.

7. Conclusion

We suggest that the total amount of crack damage induced in a rock during either heating or cooling is related to the mineral composition and most importantly the grain size and arrangement, as well as the maximum temperature that the rock has previously experienced. Hence, the apparently contradictory observations of Browning et al. (2016) and Griffiths et al. (2018) are not contradictory at all. Their observations of different patterns of cracking in different rocks appear simply to reflect the different responses of rocks with different mineralogies and microstructures to different thermal stressing regimes. We therefore suggest that

it is important to take these differences into consideration in any analysis of the evolution of crack damage processes in igneous rocks that host geothermal reservoirs or magma chambers/intrusions and hence experience cyclic changes in both stress and temperature. A priority should be to identify natural thermal memory effects in crustal rocks as such processes influence the interpretation of seismic and modeled data.

Data Availability Statement

Supporting data are included in an supporting information file and may be obtained from J. B. (email: jbrowning@ing.puc.cl) or from the NERC geoscience data center (NGDC) (<https://doi.org/10.5285/54a2032d-b626-43ad-8aa6-eb52ad7ff7ec>).

Acknowledgments

We thank the Editor Christian Huber, two anonymous reviewers, and Philip Benson for comments that helped improve the manuscript. We are grateful for continuous support from S. Boon and N. Hughes who were heavily involved with the experimental apparatus design. We thank K. Drymoni, Y. Lavallee, and F. Von Aulock for their assistance with thermal characterization of our materials. This work was partly funded by Natural Environment Research Council award NE/N002938/1, which we gratefully acknowledge. J. B. also acknowledges support from Fondecyt award 11190143 and Fondap-Conicyt 15090013.

References

- Aki, K. & Richards, P. G. (1980). *Quantitative Seismology: Theory and Methods* (p. 13). Freeman.
- Atkinson, B. K., MacDonald, D., & Meredith, P. G. (1984). Acoustic response and fracture mechanics of granite subjected to thermal and stress cycling experiments. In H. R. Hardy, Jr. & F. W. Leighton (Eds.), *Proc. Third Conf. on Acoustic Emission/Microseismic Activity in Geologic Structures and Materials* (pp. 5–18). Clausthal: Trans Tech Pub.
- Bell, A. F., Naylor, M., Heap, M. J., & Main, I. G. (2011). Forecasting volcanic eruptions and other material failure phenomena: An evaluation of the failure forecast method. *Geophysical Research Letters*, *38*, L15304. <https://doi.org/10.1029/2011GL048155>
- Benson, P. M., Austria, D. C., Gehne, S., Butcher, E., Harnett, C. E., Fazio, M., et al. (2020). Laboratory simulations of fluid-induced seismicity, hydraulic fracture, and fluid flow. *Geomechanics for Energy and the Environment*, *24*, 100169. <https://doi.org/10.1016/j.gete.2019.100169>
- Browning, J. (2015). Thermo-Mechanical Effects of Magma Chambers and Caldera Ring-Faults. Unpublished thesis, University of London.
- Browning, J., Meredith, P. G., & Gudmundsson, A. (2016). Cooling-dominated cracking in thermally stressed volcanic rocks. *Geophysical Research Letters*, *43*, 8417–8425. <https://doi.org/10.1002/2016GL070532>
- Browning, J., Meredith, P. G., Stuart, C., Harland, S., Healy, D., & Mitchell, T. M. (2017). Acoustic characterization of crack damage evolution in sandstone deformed under conventional and true triaxial loading. *Journal of Geophysical Research: Solid Earth*, *122*, 1–18. <https://doi.org/10.1002/2016JB013646>
- Browning, J., Meredith, P. G., Stuart, C., Harland, S., Healy, D., & Mitchell, T. M. (2018). A directional crack damage memory effect in sandstone under true triaxial loading. *Geophysical Research Letters*, *45*, 6878–6886. <https://doi.org/10.1029/2018GL078207>
- Burchardt, S., Tanner, D., & Krumbholz, M. (2012). The Slaufudalur pluton, southeast Iceland—An example of shallow magma emplacement by coupled cauldron subsidence and magmatic stoping. *Bulletin*, *124*(1–2), 213–227.
- Castagna, A., Ougier-Simonin, A., Benson, P. M., Browning, J., Walker, R. J., Fazio, M., & Vinciguerra, S. (2018). Thermal damage and pore pressure effects of the Brittle-Ductile transition in comiso limestone. *Journal of Geophysical Research: Solid Earth*, *123*, 7644–7660. <https://doi.org/10.1029/2017JB015105>
- Cox, S. J. D., & Meredith, P. G. (1993). Microcrack formation and material softening in rock measured by monitoring acoustic emissions. *International Journal of Rock Mechanics and Mining Science and Geomechanics Abstracts*, *30*, 11–24. [https://doi.org/10.1016/0148-9062\(93\)90172-A](https://doi.org/10.1016/0148-9062(93)90172-A)
- Fredrich, J. T., & Wong, T. (1986). Micromechanics of thermally induced cracking in three crustal rocks. *Journal of Geophysical Research*, *91*, 12,743–12,764. <https://doi.org/10.1029/JB091iB12p12743>
- Griffiths, L. (2018). *La fissuration thermique dans les roches*. Strasbourg: Doctoral dissertation.
- Griffiths, L., Lengliné, O., Heap, M. J., Baud, P., & Schmittbuhl, J. (2018). Thermal cracking in Westerly Granite monitored using direct wave velocity, coda wave interferometry, and acoustic emissions. *Journal of Geophysical Research: Solid Earth*, *123*, 2246–2261. <https://doi.org/10.1002/2017JB015191>
- Gudmundsson, A. (2006). How local stresses control magma-chamber ruptures, dyke injections, and eruptions in composite volcanoes. *Earth-Science Reviews*, *79*(1–2), 1–31. <https://doi.org/10.1016/j.earscirev.2006.06.006>
- Heap, M. J., Faulkner, D. R., Meredith, P. G., & Vinciguerra, S. (2010). Elastic moduli evolution and accompanying stress changes with increasing crack damage: Implications for stress changes around fault zones and volcanoes during deformation. *Geophysical Journal International*, *183*(1), 225–236. <https://doi.org/10.1111/j.1365-246X.2010.04726.x>
- Heap, M. J., Lavallée, Y., Laumann, A., Hess, K. U., Meredith, P. G., Dingwell, D. B., et al. (2013). The influence of thermal-stressing (up to 1000°C) on the physical, mechanical, and chemical properties of siliceous-aggregate, high-strength concrete. *Construction and Building Materials*, *42*, 248–265. <https://doi.org/10.1016/j.conbuildmat.2013.01.020>
- Heap, M. J., Vinciguerra, S., & Meredith, P. G. (2009). The evolution of elastic moduli with increasing crack damage during cyclic stressing of a basalt from Mt. Etna volcano. *Tectonophysics*, *471*, 153–160. <https://doi.org/10.1016/j.tecto.2008.10.004>
- Heimisson, E. R., Einarsson, P., Sigmundsson, F., & Brandsdóttir, B. (2015). Kilometer-scale Kaiser effect identified in Krafla volcano, Iceland. *Geophysical Research Letters*, *42*, 7958–7965. <https://doi.org/10.1002/2015GL065680>
- Holcomb, D. J. (1993). General theory of the Kaiser effect. *International Journal of Rock Mechanics and Mining Sciences & Geomechanics Abstracts*, *30*(7), 929–935. [https://doi.org/10.1016/0148-9062\(93\)90047-H](https://doi.org/10.1016/0148-9062(93)90047-H)
- Johnson, B., Gangi, A. F. & Handin, J. (1978). Thermal cracking of rock subjected to slow, uniform temperature changes, Proc. 19th U.S. Symp. Rock Mechanics, Staeline, Nevada, 259–267.
- Kaiser, J. (1953). Erkenntnisse und Folgerungen aus der Messung von Gerauschen bei Zugbeanspruchung von metallischen Werkstoffen. *Archiv Eisenhüttenwesen*, *24*, 43–45.
- Kendrick, J. E., Smith, R., Sammonds, P., Meredith, P. G., Dainty, M., & Pallister, J. S. (2013). The influence of thermal and cyclic stressing on the strength of rocks from Mount St. Helens, Washington. *Bulletin of Volcanology*, *75*(7), 728.
- Lavrov, A. (2001). Kaiser effect observation in brittle rock cyclically loaded with different loading rates. *Mechanics of Materials*, *33*(11), 669–677. [https://doi.org/10.1016/S0167-6636\(01\)00081-3](https://doi.org/10.1016/S0167-6636(01)00081-3)
- Lavrov, A. (2003). The Kaiser effect in rocks: Principles and stress estimation techniques. *International Journal of Rock Mechanics and Mining Sciences*, *40*(2), 151–171. [https://doi.org/10.1016/S1365-1609\(02\)00138-7](https://doi.org/10.1016/S1365-1609(02)00138-7)

- Lockner, D. (1993). The role of acoustic emission in the study of rock fracture. *International Journal of Rock Mechanics and Mining Sciences & Geomechanics Abstracts*, 30(7), 883–899. [https://doi.org/10.1016/0148-9062\(93\)90041-B](https://doi.org/10.1016/0148-9062(93)90041-B)
- Meredith, P. G., Knight, K. S., Boon, S. A., & Wood, I. G. (2001). The microscopic origin of thermal cracking in rocks: An investigation by simultaneous time-of-flight neutron diffraction and acoustic emission monitoring. *Geophysical Research Letters*, 28, 2105–2108. <https://doi.org/10.1029/2000GL012470>
- Miller, A. D., Julian, B. R., & Foulger, G. R. (1998). Three-dimensional seismic structure and moment tensors of non-double-couple earthquakes at the Hengill-Grensdalur volcanic complex, Iceland. *Geophysical Journal International*, 133(2), 309–325. <https://doi.org/10.1046/j.1365-246X.1998.00492.x>
- Mollo, S., Heap, M. J., Dingwell, D. B., Hess, K. U., Iezzi, G., Masotta, M., et al. (2013). Decarbonation and thermal microcracking under magmatic P-T-fco₂ conditions: The role of skarn substrata in promoting volcanic instability. *Geophysical Journal International*, 195, 369–380. <https://doi.org/10.1093/gji/ggt265>
- Nara, Y., Meredith, P. G., Yoneda, T., & Kaneko, K. (2011). Influence of macro-fractures and micro-fractures on permeability and elastic wave velocities in basalt at elevated pressure. *Tectonophysics*, 503(1–2), 52–59. <https://doi.org/10.1016/j.tecto.2010.09.027>
- Nye, J. F. (1957). *Physical Properties of Crystals* (p. 146). Oxford: Clarendon Press.
- Richter, D., & Simmons, G. (1974). Thermal expansion behaviour of igneous rocks. *International Journal of Rock Mechanics and Mining Sciences & Geomechanics Abstracts*, 15, 145–148.
- Sepúlveda, J., Arancibia, G., Molina, E., Gilbert, J. P., Duda, M., Browning, J., et al. (2020). Thermo-mechanical behavior of a granodiorite from the Liquiñe fractured geothermal system (39 S) in the Southern Volcanic Zone of the Andes. *Geothermics*, 87, 101828. <https://doi.org/10.1016/j.geothermics.2020.101828>
- Simmons, G., & Cooper, H. W. (1978). Thermal cycling cracking in three igneous rocks. *International Journal of Rock Mechanics and Mining Science and Geomechanics Abstracts*, 15, 145–148. [https://doi.org/10.1016/0148-9062\(78\)91220-2](https://doi.org/10.1016/0148-9062(78)91220-2)
- Siratovich, P. A., von Aulock, F. W., Lavallée, Y., Cole, J. W., Kennedy, B. M., & Villeneuve, M. C. (2015). Thermoelastic properties of the Rotokawa Andesite: A geothermal reservoir constraint. *Journal of Volcanology and Geothermal Research*, 301, 1–13. <https://doi.org/10.1016/j.jvolgeores.2015.05.003>
- Vinciguerra, S., Trovato, C., Meredith, P. G., & Benson, P. M. (2005). Relating seismic velocities, thermal cracking and permeability in Mt. Etna and Iceland basalts. *International Journal of Rock Mechanics and Mining Sciences*, 42, 900–910.
- Yong, C., & Wang, C.-Y. (1980). Thermally induced acoustic emission in Westerly granite. *Geophysical Research Letters*, 7, 1089–1092. <https://doi.org/10.1029/GL007i012p01089>